J. Fluid Mech. (2023), *vol*. 964, A23, doi:10.1017/jfm.2023.371

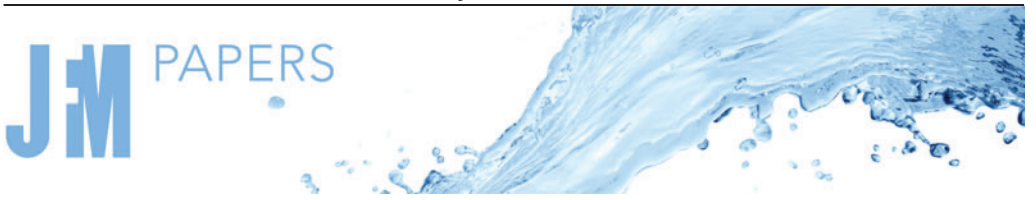

On the stability of inhomogeneous fluids under acoustic fields

Varun Kumar Rajendran[1], **S.P. Aravind Ram**[1] **and Karthick Subramani**[1],†

[1]Department of Mechanical Engineering, Indian Institute of Information Technology, Design and Manufacturing, Kancheepuram, Chennai 600127, India

(Received 13 December 2022; revised 2 May 2023; accepted 2 May 2023)

In this work, we present the stability theory for inhomogeneous fluids subjected to standing acoustic fields. Starting from the first principles, the stability criterion is established for two fluids of different acoustic impedance (product of density and speed of sound of the fluid) separated by a plane interface. Through stability theory and numerical simulations, we show that, in the presence of interfacial tension, the relocation of high-impedance fluid from the pressure anti-node to the pressure node occurs when the acoustic force overcomes the interfacial tension force, which is in agreement with recent acoustic relocation experiments in the microchannel. Furthermore, we establish an acoustic Bond number that characterizes stable ($Bo_a < 1$) and relocation ($Bo_a > 1$) regimes. Remarkably, it is found that the critical acoustic energy density required for relocation can be significantly reduced by increasing the height of the channel which could help in designing acoustofluidic devices that handle immiscible fluids.

Key words: microfluidics

1. Introduction

When an acoustic field encounters inhomogeneity, it exerts acoustic radiation force on it. Here, by inhomogeneity, we mean non-uniform or discontinuous variation of physical properties in a system such as particles/cells suspended in fluid, emulsions, co-flowing streams of miscible or immiscible fluids, and fluid subjected to a temperature gradient. The acoustic forces acting on inhomogeneity are extensively studied in microscale flows, and this field is known as 'microscale acoustofluidics' (Friend & Yeo 2011). Over the last two decades, acoustofluidics has found a wide range of applications in biological (Christakou *et al.* 2013; Collins *et al.* 2015; Iranmanesh *et al.* 2015; Ahmed *et al.* 2016; Lakshmanan *et al.* 2020), chemical (Shi *et al.* 2009; Xie *et al.* 2020) and medical (Li *et al.* 2015; Lu *et al.* 2019; Zhang *et al.* 2020) sciences.

† Email address for correspondence: karthick@iiitdm.ac.in

Recently, the relocation and stabilization of inhomogeneous co-flowing fluid streams in microchannels have gained the attention of the research community which is evident from the following works. Through silicon-glass microchannel experiments, using standing bulk acoustic waves, Deshmukh *et al.* (2014) could relocate the high-impedance sodium chloride solution to the pressure node (centre) and the low-impedance water to the pressure anti-node (sides). Also, they could stabilize a high-impedance fluid at the centre (and the low-impedance fluid to the sides) against gravity stratification using acoustic fields. Following this, using the hypothesis on mean Eulerian pressure, Karlsen, Augustsson & Bruus (2016) derived the acoustic body force to explain the relocation of inhomogeneous fluids. Using the same theory, Karlsen *et al.* (2018) showed that the acoustic body force acting on stable inhomogeneous fluid configuration could effectively suppress the boundary-driven Rayleigh streaming in the bulk. In addition to the above works on inhomogeneous miscible fluids, Hemachandran *et al.* (2019) experimentally demonstrated the relocation of immiscible fluids using acoustic fields by overcoming the interfacial tension forces. Hoque & Sen (2023) extended the analysis on immiscible fluids to study the dependence on the speed of sound, density of the fluid and the width of the fluid stream on frequency. They showed that a single resonant frequency can be achieved for the co-flowing fluids for a given width ratio. Other notable works on the practical applications of acoustic forces on co-flowing inhomogeneous fluids include iso-acoustic focusing of cells (Augustsson *et al.* 2016), acoustic focusing of sub-micron particles (Gautam *et al.* 2018; Van Assche *et al.* 2020), tweezing and patterning of inhomogeneous fluids in a microchannel (Karlsen & Bruus 2017; Baudoin *et al.* 2020), rapid mixing of fluids using an alternating multinode method (Pothuri, Azharudeen & Subramani 2019), and reversible stream–droplet transition in a microfluidic co-flowing immiscible system (Hemachandran *et al.* 2021).

In our previous work (Rajendran *et al.* 2022), the theory of acoustic forces acting on inhomogeneous fluids was developed from first principles, without any prior assumptions on the mean Eulerian pressure. The generalized acoustic body force derived was shown to predict the experimental results of Deshmukh *et al.* (2014), Karlsen *et al.* (2016), Karlsen *et al.* (2018) and Hemachandran *et al.* (2019). It was proved that an impedance gradient is a necessary condition for the relocation/stabilization of inhomogeneous fluids under acoustic fields. Nevertheless, due to the intricacy of the acoustic body force equation, the stability of a particular configuration cannot be readily inferred from it without performing numerical simulations. Although the relocation force component from the generalized acoustic body force is deduced by Rajendran *et al.* (2022), the exact conditions at which an inhomogeneous system relocates, remains stable or is neutral are not established. To address the above problem, this paper aims to provide the stability criterion (a simple algebraic equation) from which one can obtain a complete and clear picture of the stability of inhomogeneous fluids subjected to acoustic fields.

In this work, using linear stability analysis, we derive the characteristic equation that governs the stability of inhomogeneous fluids (with and without interfacial tension) under an acoustic body force. We study the various parameters such as the initial arrangement of fluids, the position of the interface with respect to the pressure node and pressure antinodes, acoustic energy density, the height of the channel or fluid interface, and surface tension to establish the necessary and sufficient conditions for relocation and stability. For fluids with interfacial tension, a non-dimensional number called the acoustic Bond number is obtained theoretically which characterizes the stable and unstable (relocation) regimes. Also, we deduce a relation between the critical acoustic energy density and the height of the channel which paves a way for relocating fluids with higher interfacial tension

($O(10^1$ mN m^{-1} to 10^2 mN m^{-1})) in a microchannel. Furthermore, numerical simulations are carried out using a generalized acoustic body force which agrees well with the derived theoretical stability criterion.

2. Physics of the problem

The hydrodynamics of the inhomogeneous fluids involved in this study is governed by the mass-continuity and momentum equations (Landau & Lifshitz 1987),

$$\frac{\partial \rho}{\partial t} + \boldsymbol{\nabla} \cdot (\rho \boldsymbol{V}) = 0, \tag{2.1a}$$

$$\rho \frac{\mathrm{D}\boldsymbol{V}}{\mathrm{D}t} = -\boldsymbol{\nabla} p + \eta \nabla^2 \boldsymbol{V} + \beta \eta \boldsymbol{\nabla}(\boldsymbol{\nabla} \cdot \boldsymbol{V}) + \boldsymbol{f}_{ac}, \tag{2.1b}$$

where ρ represents density, $\boldsymbol{V}$ represents the velocity vector field, p represents the pressure field, η is the dynamic viscosity of the fluid, $\beta = (\xi/\eta) + (1/3)$, ξ is the bulk viscosity, $\mathrm{D}/\mathrm{D}t$ denotes the material derivative ($\mathrm{D}/\mathrm{D}t = \partial_t + \boldsymbol{V} \cdot \boldsymbol{\nabla}$) and all the above fields vary at a slow time scale t.

The body force $\boldsymbol{f}_{ac}$ responsible for the above slow time scale phenomena is created by the acoustic fields varying at a fast time scale (t_f). In general, the dependent fields such as velocity, pressure, density and compressibility can be decomposed using perturbation theory, based on the time scales as $g_\tau = g(\boldsymbol{r}, t) + g_1(\boldsymbol{r}, t_f)$, where $g_1(\boldsymbol{r}, t_f) = g_1(\boldsymbol{r})\mathrm{e}^{-\mathrm{i}\omega t_f}$ is a first-order time-harmonic acoustic field that varies on the fast time scale t_f ($t_f \sim 1/\omega \sim 0.1\ \mu$s), $\omega(\sim 1$ MHz) is the angular frequency of the acoustic fields and g is the fields that vary on a slow time scale $t(t \gg t_f)$. The slow time scale phenomena such as acoustic streaming, acoustic relocation and streaming suppression are created by $\boldsymbol{f}_{ac}$ which is the divergence of the time-averaged Reynolds stress tensor consisting of the product of first-order fast time scale acoustic fields (Rajendran *et al.* 2022),

$$\begin{aligned}\boldsymbol{f}_{ac} = -\boldsymbol{\nabla} \cdot \langle \rho \boldsymbol{v}_1 \boldsymbol{v}_1 \rangle &= \left(\tfrac{1}{2}\boldsymbol{\nabla}(\kappa \langle |p_1|^2 \rangle - \rho \langle |\boldsymbol{v}_1|^2 \rangle)\right) + (\langle \boldsymbol{v}_1 \times \boldsymbol{\nabla} \times (\rho \boldsymbol{v}_1) \rangle) \\ &\quad + \left(-\tfrac{1}{2}\langle |p_1|^2 \rangle \boldsymbol{\nabla}\kappa - \tfrac{1}{2}\langle \boldsymbol{v}_1^2 \rangle \boldsymbol{\nabla}\rho\right) \qquad (2.2) \\ &= (\boldsymbol{f}_{ac_1}) + (\boldsymbol{f}_{ac_2}) + (\boldsymbol{f}_{ac_3}), \qquad (2.3)\end{aligned}$$

where p_1 and $\boldsymbol{v}_1$ denote the first-order (fast time scale) pressure and velocity fields due to acoustic waves (see Appendix A) and $\langle \cdots \rangle$ indicates time averaging over a period $t \gg t_f$ (the time average of two first-order fields $\langle \boldsymbol{u}_1 \boldsymbol{v}_1 \rangle$ is defined as $\frac{1}{2}\mathrm{Re}(\boldsymbol{u}_1^\star \boldsymbol{v}_1)$, where $\star$ denotes complex conjugation). The terms ρ and κ denote the slow time scale (background) density and compressibility of the fluid respectively. In (2.2), the first term ($\boldsymbol{f}_{ac_1}$) is a conservative or gradient term that induces pressure and not fluid flow, the second term ($\boldsymbol{f}_{ac_2}$) is only dominant at boundary layers and is responsible for boundary-driven Rayleigh streaming, and the third term ($\boldsymbol{f}_{ac_3}$) is responsible for relocation and stabilization of inhomogeneous fluids. Hence, only the relevant third term, $\boldsymbol{f}_{ac_3}$, is considered for theoretical analysis. For the standing acoustic wave applied along the x-direction, the pressure $p_1 = p_a \sin(k_w x)$ and velocity $\boldsymbol{v}_1 = (p_a/i\rho c)\cos(k_w x)$, where p_a denotes the pressure amplitude, c denotes the speed of sound in a medium, $k_w = 2\pi/\lambda_w$ denotes the wavenumber, λ_w denotes the wavelength (for standing half-wave, $\lambda_w = 2w$, where w is the width of the channel). The force term $\boldsymbol{f}_{rl}$ causing the relocation can be obtained from $\boldsymbol{f}_{ac_3}$ after disregarding

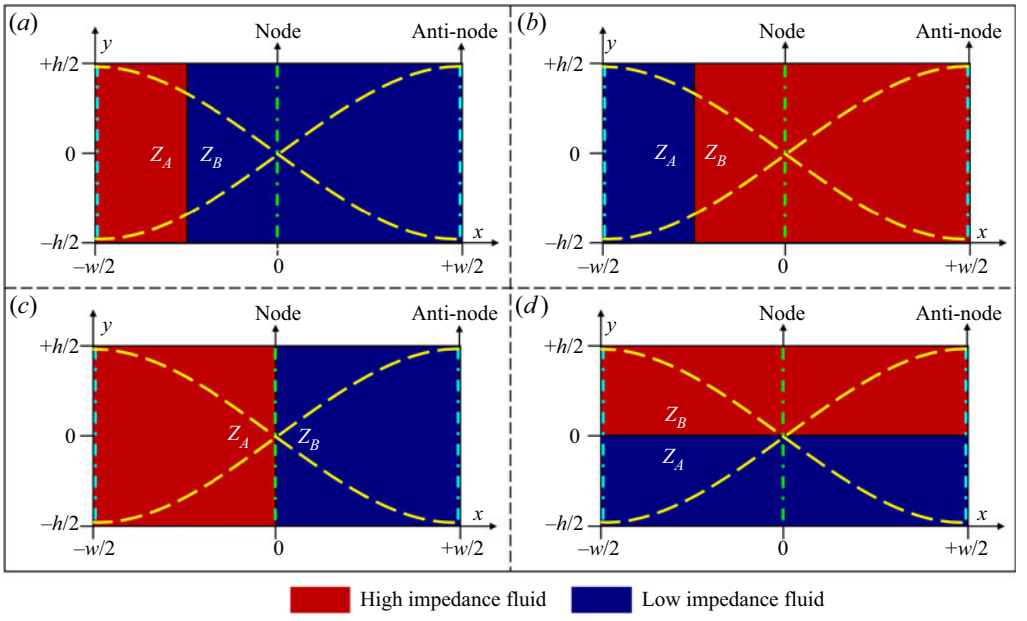

Figure 1. Inhomogeneous fluids (of different impedance Z_A and Z_B) separated by a plane interface subjected to a standing acoustic half-wave. In the absence of interfacial tension, the fluid system (*a*) is in an unstable equilibrium, (*b*) is in a stable equilibrium, (*c*) is in neutral equilibrium and (*d*) is in a non-equilibrium state. In the presence of interfacial tension, the fluid system (*a*) is in a conditionally stable equilibrium, (*b*) is in stable equilibrium, (*c*) is in stable equilibrium and (*d*) is in a conditionally stable equilibrium. Note: (*d*) the configuration shown is not in the scope of this work.

the conservative term, which can be written as (Rajendran *et al.* 2022)

$$\boldsymbol{f}_{rl} = -E_{ac}\cos(2k_w x)\nabla\tilde{Z}, \tag{2.4}$$

where $E_{ac} = p_a^2/(4\rho_{avg}c_{avg}^2) = (v_a^2\rho_{avg})/4$ is the acoustic energy density, v_a denotes the velocity amplitude, $Z = \rho c$ denotes impedance, $\tilde{Z} = Z/Z_{avg}$, $\tilde{c} = c/c_{avg}$ and $\tilde{\rho} = \rho/\rho_{avg}$, where the subscript 'avg' denotes the respective average quantities of fluids A and B. Here, $x = 0$ denotes the pressure node and $x = \pm w/2$ denote the pressure anti-nodes. To improve readability, throughout the manuscript, 'pressure node' and 'pressure anti-nodes' are referred to as 'node' and 'anti-node' respectively. It is important to note that the first-order fields p_1 and v_1 assumed for the theoretical analysis correspond to a homogeneous fluid. However, an inhomogeneous fluid configuration of different fluid impedances (Z_A and Z_B) leads to different pressure fields and different acoustic wavelengths in the two fluids. The accuracy of this assumption is evaluated using numerical simulations in § 3.2, where the variation of the pressure field in each fluid is taken into account.

2.1. *Stability analysis of inhomogeneous fluids in the absence of interfacial tension*

A two-dimensional fluid domain subjected to a standing acoustic half-wave in the x-direction, with two fluids separated by a sharp vertical interface, as shown in figure 1(*a–c*), is considered for the stability analysis. Before beginning the analysis, it is necessary to understand the equilibrium of the system in the absence of interfacial tension. In a completely enclosed domain, a fluid initially at rest ($V = 0$) will remain at rest (or equilibrium) if the body force can be completely absorbed in pressure, $\boldsymbol{f}_{rl} = \nabla p$ from

(2.1*b*) and (2.4). By taking the curl of the above relation, the condition for equilibrium is given as $\boldsymbol{\nabla} \times \boldsymbol{f}_{rl} = 0$. Thus,

$$-\frac{E_{ac}}{Z_{avg}}\left[\frac{\partial}{\partial x}\left(\cos(2k_w x)\frac{\partial Z}{\partial y}\right) - \frac{\partial}{\partial y}\left(\cos(2k_w x)\frac{\partial Z}{\partial x}\right)\right] = 0. \tag{2.5}$$

It is clear from (2.5) that the given fluid configuration will be in an equilibrium state, only if the direction of the acoustic standing wave is normal to the fluid–fluid interface (the direction of the acoustic standing wave is parallel to the direction of the impedance gradient) as shown in figures 1(*a*)–1(*c*). Since $\boldsymbol{\nabla} \times \boldsymbol{f}_{rl} \neq 0$ for the configuration shown in figure 1(*d*), it is not in equilibrium and tends to relocate to the stable configuration without any perturbations. The stability nature of the equilibrium configurations is analysed by imposing infinitesimal perturbations on the interface. Now we proceed to show that in the absence of interfacial tension, the configuration shown in figure 1(*a*) is in unstable equilibrium (perturbations grow), figure 1(*b*) is in stable equilibrium (perturbations decay) and figure 1(*c*) is in neutral equilibrium (perturbations neither grow nor decay).

The effect of viscosity is neglected in the stability analysis, as it governs only the time scale of the phenomenon and does not contribute to the stability criterion. Although the physical properties are non-uniform in an inhomogeneous system, the fluid particles considered in the flow field have constant density ρ, speed of sound c and impedance Z. Thus, the material derivative of all properties is zero, which includes the incompressibility condition ($\mathrm{D}\rho/\mathrm{D}t = \partial\rho/\partial t + \boldsymbol{V}\cdot\boldsymbol{\nabla}\rho = 0$). By combining the incompressibility condition with (2.1*a*) and neglecting the viscosity, the governing equations (2.1) reduce to

$$\frac{\partial u}{\partial x} + \frac{\partial v}{\partial y} = 0, \tag{2.6a}$$

$$\rho\frac{\mathrm{D}u}{\mathrm{D}t} = -\frac{\partial p}{\partial x} - \frac{E_{ac}\cos(2k_w x)}{Z_{avg}}\frac{\partial Z}{\partial x}, \tag{2.6b}$$

$$\rho\frac{\mathrm{D}v}{\mathrm{D}t} = -\frac{\partial p}{\partial y} - \frac{E_{ac}\cos(2k_w x)}{Z_{avg}}\frac{\partial Z}{\partial y}, \tag{2.6c}$$

where u, v are the x-component and y-component of the velocity field $\boldsymbol{V}$. Since the body force term is a function of impedance, the following impedance relation is required for the closure:

$$\frac{\mathrm{D}Z}{\mathrm{D}t} = \frac{\partial Z}{\partial t} + u\frac{\partial Z}{\partial x} + v\frac{\partial Z}{\partial y} = 0. \tag{2.6d}$$

Now, the flow fields are decomposed into an unperturbed zeroth-order stationary state and infinitesimal perturbations as $u = u_0 + \delta u$, $v = v_0 + \delta v$, $p = p_0 + \delta p$, $\rho = \rho_0 + \delta\rho$ and $Z = Z_0 + \delta Z$. In this study, the variation of acoustic impedance is considered only in the x-direction (figure 1*a–c*), $Z_0 = Z_0(x)$. At the stationary state ($u_0 = v_0 = 0$), the unperturbed zeroth-order equations become $\partial p_0/\partial x = -(E_{ac}\cos(2k_w x)/z_{avg})(\partial Z_0/\partial x)$ from (2.6*b*), $\partial p_0/\partial y = 0$ from (2.6*c*) and $\partial Z_0/\partial t = 0$ from (2.6*d*). Using the above zeroth-order relations and neglecting the second-order terms in (2.6), the first-order

perturbation equations governing the stability become

$$\frac{\partial \delta u}{\partial x} + \frac{\partial \delta v}{\partial y} = 0, \tag{2.7a}$$

$$\rho_0 \frac{\partial \delta u}{\partial t} = -\frac{\partial \delta p}{\partial x} - \frac{E_{ac}\cos(2k_w x)}{Z_{avg}} \frac{\partial \delta Z}{\partial x}, \tag{2.7b}$$

$$\rho_0 \frac{\partial \delta v}{\partial t} = -\frac{\partial \delta p}{\partial y} - \frac{E_{ac}\cos(2k_w x)}{Z_{avg}} \frac{\partial \delta Z}{\partial y}, \tag{2.7c}$$

$$\frac{\partial (\delta Z)}{\partial t} = -\delta u \frac{\partial Z_0}{\partial x}. \tag{2.7d}$$

Analysing the disturbances into normal modes, the amplitude of the disturbances δu, δv, $\delta \rho$, δp and δz takes the following form:

$$A(x, y, t) = \hat{A}(x)\exp(\mathrm{i}k_y y + nt), \tag{2.8}$$

where k_y is the wavenumber considered along the y-direction. Applying the above amplitude relations in the form of (2.8) to (2.7),

$$\frac{\partial \widehat{\delta u}}{\partial x} + \mathrm{i}k_y \widehat{\delta v} = 0, \tag{2.9a}$$

$$\rho_0 n \widehat{\delta u} = -\frac{\partial \widehat{\delta p}}{\partial x} - \frac{E_{ac}\cos(2k_w x)}{Z_{avg}} \frac{\partial \widehat{\delta Z}}{\partial x}, \tag{2.9b}$$

$$\rho_0 n \widehat{\delta v} = -\mathrm{i}k_y \widehat{\delta p} - \mathrm{i}k_y \frac{E_{ac}\cos(2k_w x)}{Z_{avg}} \widehat{\delta Z}, \tag{2.9c}$$

$$n \widehat{\delta Z} = -\widehat{\delta u} \frac{\partial Z_0}{\partial x}. \tag{2.9d}$$

The partial notation is dropped since the only derivatives in (2.9) are with respect to the x coordinate. Multiplying by $\mathrm{i}k_y$ throughout (2.9c) and combining with (2.9a) and (2.9d), we obtain

$$\widehat{\delta p} = -\rho_0 \frac{n}{{k_y}^2} \frac{\mathrm{d}\widehat{\delta u}}{\mathrm{d}x} + E_{ac} \frac{\cos(2k_w x)}{Z_{avg}} \frac{\widehat{\delta u}}{n} \frac{\mathrm{d}Z_0}{\mathrm{d}x}. \tag{2.10}$$

Substituting (2.9d) and (2.10) into (2.9b) results in

$$\frac{\mathrm{d}}{\mathrm{d}x}\left(\rho_0 \frac{\mathrm{d}\widehat{\delta u}}{\mathrm{d}x}\right) - \rho_0 k_y^2 \widehat{\delta u} = -E_{ac} \frac{2k_w \widehat{\delta u}}{Z_{avg}} \frac{k_y^2}{n^2} \frac{\mathrm{d}Z_0}{\mathrm{d}x} \sin(2k_w x). \tag{2.11}$$

Considering two uniform fluids of different impedance Z_A and Z_B separated by interfaces positioned at x_s,

$$Z_0 = Z_A + (Z_B - Z_A)H(x - x_s), \tag{2.12a}$$

$$\frac{\mathrm{d}Z_0}{\mathrm{d}x} = (Z_B - Z_A)\delta(x - x_s), \tag{2.12b}$$

where $H(x - x_s)$ is the Heaviside step function at $x = x_s$ and $\delta(x - x_s)$ is Dirac's δ-function at $x = x_s$. Substituting (2.12b) into (2.11),

$$\frac{\mathrm{d}}{\mathrm{d}x}\left(\rho_0 \frac{\mathrm{d}\widehat{\delta u}}{\mathrm{d}x}\right) - \rho_0 k_y^2 \widehat{\delta u} = -E_{ac} \frac{2k_w \widehat{\delta u}}{Z_{avg}} \frac{k_y^2}{n^2} \sin(2k_w x)(Z_B - Z_A)\delta(x - x_s). \tag{2.13}$$

Equation (2.13) is the governing differential equation for the stability of inhomogeneous fluids (without interfacial tension). For a uniform region on either side of the interface(s) where there are no discontinuities in the impedance, the governing equation (2.13) reduces to

$$\frac{\mathrm{d}^2\widehat{\delta u}}{\mathrm{d}x^2} - k_y^2\widehat{\delta u} = 0. \tag{2.14}$$

The solution of (2.14) is of the form $\widehat{\delta u} = C_1\exp(k_y(x-x_s)) + C_2\exp(-k_y(x-x_s))$, where C_1, C_2 are constants. Since $\widehat{\delta u}$ must vanish at the boundaries, we can write the solution as

$$\widehat{\delta u}_B = C\exp(k_y(x-x_s)) \quad (x < x_s), \tag{2.15a}$$

$$\widehat{\delta u}_A = C\exp(-k_y(x-x_s)) \quad (x > x_s), \tag{2.15b}$$

where the constant C in (2.15) is chosen to ensure continuity in velocity across the interfaces. For the solution at the interface ($x = x_s$), we integrate (2.13) along infinitesimal distance ($\mathrm{d}x \approx 0$), the second term in the left-hand side of the equation is zero and the remaining terms are

$$\Delta\left(\rho_0\frac{\mathrm{d}\widehat{\delta u_s}}{\mathrm{d}x}\right) = -E_{ac}\frac{2k_w\widehat{\delta u_s}}{Z_{avg}}\frac{k_y^2}{n^2}(Z_B - Z_A)\int(\sin(2k_w x)\delta(x-x_s))\,\mathrm{d}x, \tag{2.16}$$

where $\widehat{\delta u_s}$ is the value of $\widehat{\delta u}$ at $x = x_s$. Using (2.15) and the Dirac delta identity $\int f(x)\delta(x-a)\,\mathrm{d}x = f(a)$ to solve for eigenvalue n in (2.16),

$$\rho_A(-k_y\widehat{\delta u_s}) - \rho_B(k_y\widehat{\delta u_s}) = -E_{ac}\frac{2k_w\widehat{\delta u_s}}{Z_{avg}}\frac{k_y^2}{n^2}(Z_B - Z_A)\sin(2k_w x_s), \tag{2.17}$$

where ρ_A and ρ_B indicate the densities of fluids A and B. Rearranging (2.17), the characteristic value n for the stability problem becomes

$$n = \sqrt{\frac{k_y}{\rho_A + \rho_B}\phi E_{ac}(Z_B - Z_A)\sin(2k_w x_s)}, \tag{2.18}$$

where $\phi = 2k_w/Z_{avg}$. From the above characteristic value n, the slow time scale $t \sim 1/n \sim$ 1 ms (as $k_w, k_y \sim O(10^4)$, $E_{ac} \sim O(10^2)$, $\rho \sim O(10^3)$, $c \sim O(10^3)$, $\omega \sim O(10^6)$ and $Z \sim O(10^6)$), which is much greater than the fast time scale acoustic fields $t_f \sim 1/\omega \sim 0.1\ \mu$s.

The characteristic equation (2.18) establishes the acoustic stability criterion when inhomogeneous fluids (without interfacial tension) in a microchannel are subjected to a standing acoustic wave. If the eigenvalue n is imaginary in (2.18), then the configuration is in a stable equilibrium and the configuration is in an unstable equilibrium when the eigenvalue n is real. For a standing acoustic half-wave, in (2.18), the values of $k_y/(\rho_B + \rho_A)$, ϕ and E_{ac} are always positive. Thus, the sign of $Z_B - Z_A$ (initial configuration of the fluids) and $\sin(2k_w x_s)$ (relative location of the interface with respect to the standing acoustic wave) decide the nature of the eigenvalue in (2.18). Here, $Z_B - Z_A$ is positive when high-impedance fluid is present to the right of the interface and negative when high-impedance fluid is present to the left of the interface. Additionally, $\sin(2k_w x_s)$ has a negative value to the left of the node (x_s is negative), a positive value to the right of the node (x_s is positive) and zero when the interface coincides with the node (centre of the microchannel) or anti-node (sides of the microchannel) ($x_s = 0$).

(*a*)

(i)

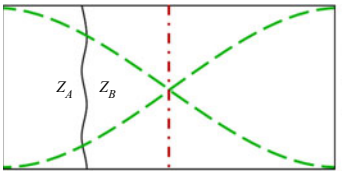

Condition	$\sin(2k_w x_s)$	$Z_B - Z_A$	Fluids without interfacial tension		Fluids with interfacial tension	
			n	Nature of the system	n	Nature of the system
$Z_A < Z_B$	–	+	$\sqrt{-}$	Always stable	$\sqrt{-}$	Always stable
$Z_A > Z_B$	–	–	$\sqrt{+}$	Always unstable	$\sqrt{-}$	Stable when $E_{ac} < E_{cr}$
					$\sqrt{+}$	Unstable when $E_{ac} > E_{cr}$

(ii)

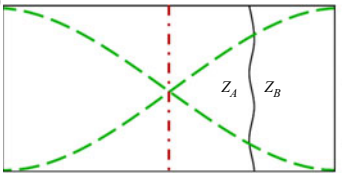

Condition	$\sin(2k_w x_s)$	$Z_B - Z_A$	Fluids without interfacial tension		Fluids with interfacial tension	
			n	Nature of the system	n	Nature of the system
$Z_A < Z_B$	+	+	$\sqrt{+}$	Always unstable	$\sqrt{-}$	Stable when $E_{ac} < E_{cr}$
					$\sqrt{+}$	Unstable when $E_{ac} > E_{cr}$
$Z_A > Z_B$	+	–	$\sqrt{-}$	Always stable	$\sqrt{-}$	Always stable

(iii)

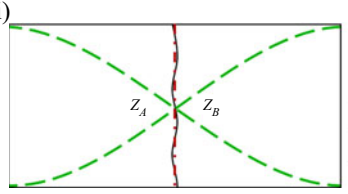

Condition	$\sin(2k_w x_s)$	$Z_B - Z_A$	Fluids without interfacial tension		Fluids with interfacial tension	
			n	Nature of the system	n	Nature of the system
$Z_A < Z_B$	0	+	0	Neutral equilibrium	$\sqrt{-}$	Always stable
$Z_A > Z_B$	0	–				

(*b*)

(i)

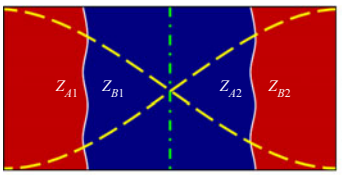

Condition	$\sin(2k_w x_s)$	$Z_B - Z_A$	Fluids without interfacial tension		Fluids with interfacial tension	
			n	Nature of the system	n	Nature of the system
IF_1: $Z_{A1} > Z_{B1}$	–	–	$\sqrt{+}$	Always unstable	$\sqrt{-}$	Stable when $E_{ac} < E_{cr}$
					$\sqrt{+}$	Unstable when $E_{ac} > E_{cr}$
IF_2: $Z_{A2} < Z_{B2}$	+	+	$\sqrt{+}$	Always unstable	$\sqrt{-}$	Stable when $E_{ac} < E_{cr}$
					$\sqrt{+}$	Unstable when $E_{ac} > E_{cr}$

(ii)

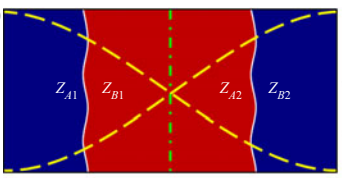

Condition	$\sin(2k_w x_s)$	$Z_B - Z_A$	Fluids without interfacial tension		Fluids with interfacial tension	
			n	Nature of the system	n	Nature of the system
IF_1: $Z_{A1} < Z_{B1}$	–	–	$\sqrt{-}$	Always stable	$\sqrt{-}$	Always stable
IF_2: $Z_{A2} > Z_{B2}$	+	+	$\sqrt{-}$	Always stable	$\sqrt{-}$	Always stable

High impedance fluid Low impedance fluid

Figure 2. Different inhomogeneous fluid configurations commonly used in microfluidics and their equilibrium nature. (*a*) Single interface configurations; (*b*) double interface configurations. Equations (2.18) and (2.21) are used to calculate n for fluids without interfacial tension and with interfacial tension.

As per the above arguments, the inhomogeneous system in figure 1(*a*) is in an unstable equilibrium as eigenvalue n is real, and the system in figure 1(*b*) is in a stable equilibrium as eigenvalue n is imaginary. It can be concluded from the above discussion and figures 2(*a*-i) and 2(*a*-ii) that a system is said to be acoustically stable (unstable) if the initial configuration of the fluids is in such a way that the low (high) impedance fluid is present at the anti-node(s) and the high (low) impedance fluid is present at the node(s). This conclusion is consistent with the demonstration of acoustic relocation of fluids within a microchannel by Deshmukh *et al.* (2014). For the case where the interface coincides with the node, $\sin(2k_w x_s) = 0$. Thus, the system is in a neutral equilibrium ($n = 0$) as shown in figures 1(*c*) and 2(*a*-iii). The above analysis can be easily extended to an inhomogeneous

system consisting of multiple interfaces. In this case, the eigenvalues evaluated at the fluid interfaces govern the nature of the system. Figure 2(*b*) shows the stability of two interface systems that are widely used in acoustofluidic applications (Augustsson *et al.* 2016; Karthick & Sen 2018; Nath & Sen 2019; Wu *et al.* 2019; Rufo *et al.* 2022). It can be seen from figure 2(*b*-i) that when high impedance fluid is at the sides (anti-nodes), the eigenvalue at both the interfaces (IF_1 and IF_2) is real and hence the system is in unstable equilibrium. The system is in stable equilibrium in figure 2(*b*-ii), as the eigenvalue at both interfaces is imaginary.

2.2. *Stability analysis of inhomogeneous fluids in the presence of interfacial tension*

Proceeding to solve for immiscible fluids, the effect of surface tension must be accounted. The discontinuity in impedance occurring in the interfaces (x_s) is modelled by including the interfacial tension effects in the x momentum equation (2.9*b*) as (Chandrasekhar 1961)

$$\rho_0 n\widehat{\delta u} = -\frac{\partial\widehat{\delta p}}{\partial x} - \frac{E_{ac}\cos(2k_w x)}{Z_{avg}}\frac{\partial\widehat{\delta Z}}{\partial x} - k_y^2\sum_s T\widehat{\delta x_s}\delta(x-x_s), \tag{2.19}$$

where T is the interfacial tension and $\widehat{\delta x_s}$ denotes the perturbation of the interfaces, and $(\mathrm{d}/\mathrm{d}t)\widehat{\delta x_s} = \widehat{\delta u_s} \implies \widehat{\delta x_s} = \widehat{\delta u_s}/n$. The governing differential equation for stability between inhomogeneous fluids with interfacial tension is obtained similar to the case without interfacial tension, as in § 2.1,

$$\frac{\mathrm{d}}{\mathrm{d}x}\left(\rho_0\frac{\mathrm{d}\widehat{\delta u}}{\mathrm{d}x}\right) - \rho_0 k_y^2\widehat{\delta u} = -E_{ac}\frac{2k_w\widehat{\delta u}}{Z_{avg}}\frac{k_y^2}{n^2}\sin(2k_w x)(Z_B - Z_A)\delta(x-x_s) + \frac{k_y^2}{n^2}\sum_s k_y^2\left(T\widehat{\delta u_s}\right)\delta(x-x_s). \tag{2.20}$$

Integrating (2.20) across an infinitesimal distance ($\mathrm{d}x \approx 0$) and solving for the characteristic value n,

$$n = \sqrt{\frac{k_y}{\rho_A+\rho_B}\left(\phi E_{ac}(Z_B - Z_A)\sin(2k_w x_s) - k_y^2 T\right)}. \tag{2.21}$$

From the above characteristic equation for n, the slow time scale t is ($\sim 1/n \sim 1$ ms, where $T \sim O(10^{-3})$) is much greater than the fast time scale acoustic fields ($t_f \sim 0.1$ µs). Equation (2.21) establishes the acoustic stability criterion when fluids with interfacial tension are subjected to a standing acoustic wave. It can be seen from (2.21) that the interfacial tension (T) and wavenumber of the perturbation (k_y) play a role in the stability of immiscible fluids.

In the presence of interfacial tension ($T > 0$), the fluid system shown in figure 1(*b*) is always stable, as the negative sign of $(Z_B - Z_A)\sin(2k_w x_s)$ results in an imaginary eigenvalue n in (2.21). However, for the fluid system shown in figure 1(*a*), the sign of $(Z_B - Z_A)\sin(2k_w x_s)$ is positive in (2.21). Thus, the system is conditionally stable, and the stability is determined by the relative magnitudes of $\phi E_{ac}(Z_B - Z_A)\sin(2k_w x_s)$ and $k_y^2 T$. The fluid system in figure 1(*a*) becomes unstable (n is real) if the acoustic force density F_{rl} ($\phi E_{ac}(Z_B - Z_A)\sin(2k_w x_s)$) dominates (or is greater than) the interfacial force density F_{int} ($k_y^2 T$) and becomes stable (n is imaginary) if the interfacial force density dominates the acoustic force density. For the case where the interface coincides with the

node ($\sin(2k_w x_s) = 0$ and eigenvalue n is imaginary), the system is in a stable equilibrium, as shown in figures 1(*c*) and 2(*a*-iii).

Now, for a conditionally stable configuration, we proceed to find the minimum energy density required to relocate the fluid systems in figures 1(*a*) and 2(*b*-i) with interfacial tension ($T > 0$). Since the interface height, h, is finite, this leads to the quantization of the possible modes $k_y = k_{h_m} = m\pi/h$. The minimum (critical) acoustic energy density (E_{cr}) required to relocate the fluid system is decided by the first conceivable mode, $k_{h_1} = k_h = \pi/h$, and the critical acoustic energy density is obtained by limiting the eigenvalue n to zero in (2.21). Thus,

$$E_{cr} = \frac{k_h^2 T Z_{avg}}{\sin(2k_w x_s) 2k_w (Z_B - Z_A)}. \tag{2.22}$$

If the applied energy density E_{ac} is less than the critical energy density E_{cr} ($E_{ac} < E_{cr}$), the interfacial tension succeeds in stabilizing a potentially unstable configuration. The same system becomes unstable and eventually relocates to a stable configuration when $E_{ac} > E_{cr}$, which qualitatively agrees with the recent experiments by Hemachandran *et al.* (2019). The above discussions on the equilibrium nature of different inhomogeneous fluid configurations (with and without interfacial tension) are clearly summarized in figure 2.

3. Numerical results and discussion

The numerical framework employed here is similar to the previous work (Rajendran *et al.* 2022). At first, we study the stability and relocation using the acoustic relocation force $\boldsymbol{f}_{rl}$ in (2.4) where the acoustic energy density is assumed to be constant. In addition to this, we extend the numerical analysis using the generalized acoustic body force $\boldsymbol{f}_{ac}$ in (2.2) where the first-order pressure and velocity vary during relocation (thus E_{ac} is time-dependent) (Rajendran *et al.* 2022).

The numerical analysis is carried out on a two-dimensional fluid domain of height $h = 160$ μm and width $w = 360$ μm in COMSOL Multiphysics 6.0. Along with the laminar flow equations, the discontinuous interface used in the theoretical analysis is modelled as sharp but continuous using phase field equations. For this study, the fluids mineral oil ($Z = 1.23$ MPa s m^{-1}) and silicone oil ($Z = 0.961$ MPa s m^{-1}) are used. A mesh refinement procedure, similar to those employed by Rajendran *et al.* (2022), is used to confirm that the numerical findings are not affected by grid size. Three different fluid configurations are considered for the study, namely:

(i) High–Low–High (HLH) configuration where the high impedance fluid is present at the anti-nodes (sides) and the low impedance fluid is present at the node (centre) as shown in figure 3(*a*);
(ii) Low–High–Low (LHL) configuration where the low impedance fluid is present at the anti-nodes (sides) and the high impedance fluid is present at the node (centre) as shown in figure 3(*b*);
(iii) High–Low (HL) configuration where the high impedance fluid occupies the domain to the left of the centre of the microchannel and the low impedance fluid occupies the domain to the right of the centre of the microchannel as shown in figure 3(*c*).

For the sake of brevity, the configurations shown in figures 2(*a*-i) (or 1) and 2(*a*-ii) are not discussed explicitly as their stability and relocation are captured by the HLH and LHL configurations. The Low–High (LH) configuration is also not discussed, as it would be

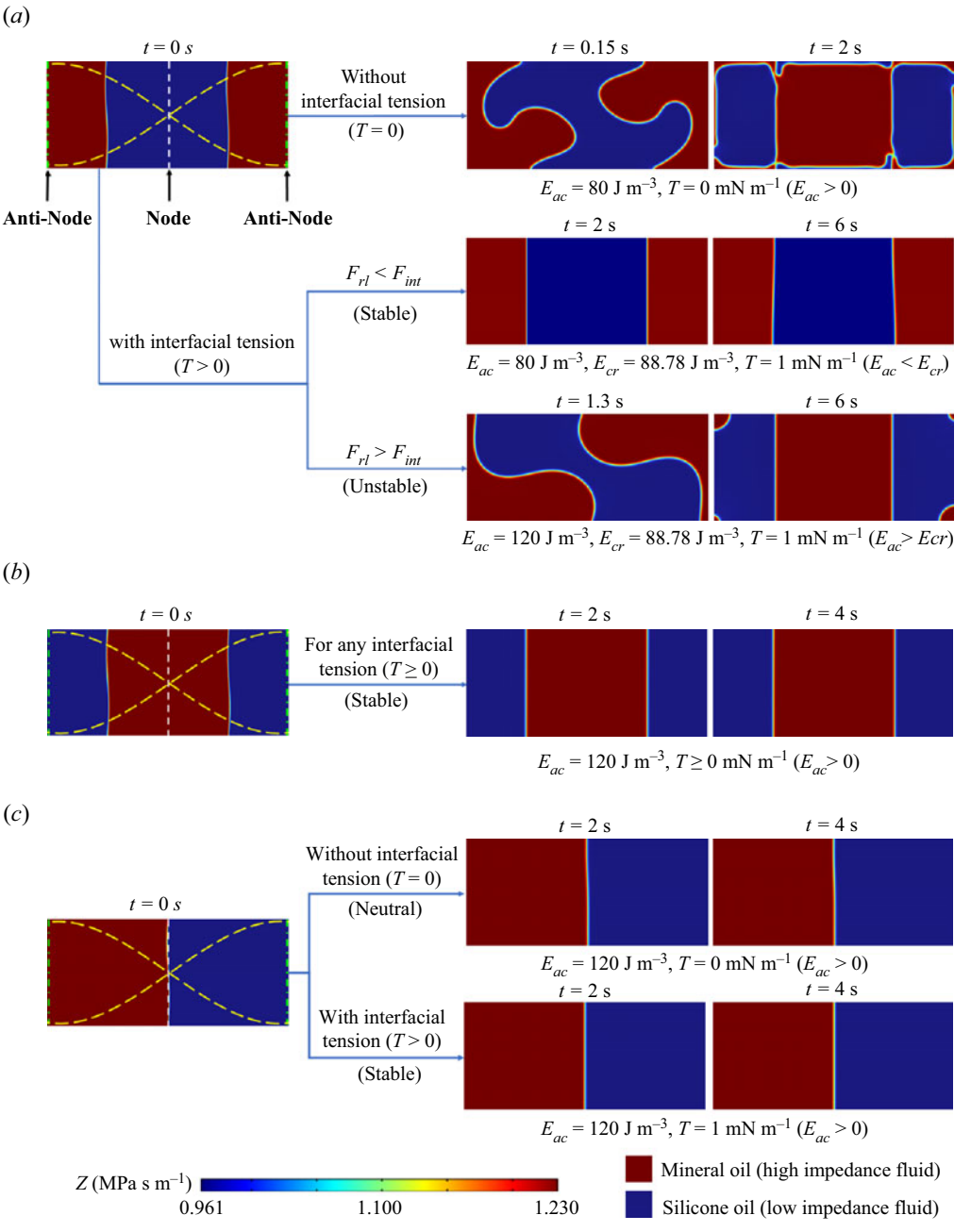

Figure 3. Stabilization and relocation of inhomogeneous fluids using simplified body force (2.4) with constant E_{ac}: (*a*) HLH configuration; (*b*) LHL configuration; (*c*) HL configuration.

analogous to the HL configuration. For all the analyses, the initial interface is perturbed and modelled as $x_s(y) = A_0 \cos((2\pi/h)y + h/2)$, where $A_0 = 0.01h$ is the perturbation amplitude.

3.1. *Numerical analysis of stability using relocation body force f_{rl} and steady acoustic energy density E_{ac}*

For the numerical simulations shown in figure 3, we employ (2.4) as body force and assume E_{ac} to be constant with respect to time, throughout the relocation process. The boundary condition for the analysis is no slip at the walls and the pressure is constrained at a point (bottom left corner of the channel). In the absence of interfacial tension ($T = 0$ mN m^{-1}), it is observed that for any $E_{ac} > 0$, the HLH configuration undergoes relocation to a stable LHL configuration as in figure 3(a) (the simulation is shown for $E_{ac} = 80$ J m^{-3}). In this case, the magnitude of E_{ac} only influences the time scale of the relocation process by competing with the viscosity. However, in the presence of interfacial tension, $T = 1$ mN m^{-1}, the HLH fluid configuration remained stable for all energy densities below 88 J m^{-3}, and relocation is observed for all energy densities above 89 J m^{-3}. These simulations are in close agreement with the critical acoustic energy density $E_{cr} = 88.78$ J m^{-3} predicted by (2.22) for the mineral–silicone oil combination. Simulation results of other fluid combinations shown in figure 5 also agree with (2.22). When the applied E_{ac} is just above E_{cr}, the fluids take a much longer time to relocate. Thus, for convenience, the simulation is shown for $E_{ac} = 120$ J m^{-3} in figure 3(a).

For LHL configuration with and without interfacial tension ($T \geq 0$), for any $E_{ac} > 0$, the relocation of fluid is not observed, and the system remained stable, as shown in figure 3(b) (the simulation is shown for $E_{ac} = 120$ J m^{-3}). In the HL configuration, the node of the standing acoustic half-wave coincides with the fluid–fluid interface. Here, for fluids with interfacial tension, relocation is not observed for any $E_{ac} > 0$ and the fluid system remained stable (figure 3c). However, for fluids without interfacial tension, the HL configuration is observed to be in neutral equilibrium (figure 3c). These simulation results of unstable, stable and neutral equilibrium of inhomogeneous fluids (figure 3) are in agreement with the stability criteria (from (2.18) and (2.21)) that we established theoretically in § 2.

The applicability of the steady E_{ac} assumption on the relocation of larger impedance difference fluids is discussed below. The resonant frequency changes as the fluid distribution varies inside the channel during the relocation process. Thus, when the system is actuated at a single frequency, E_{ac} is stronger for some resonant intermediate configurations and drops drastically for most of the non-resonant intermediate configurations. In our previous work (Jayakumar & Subramani 2022), this problem is overcome using the frequency sweep between the resonant frequencies of stable and unstable configurations. In this way, E_{ac} does not vary significantly and can be maintained approximately constant during the relocation process. This clearly demonstrates the relevance of the steady E_{ac} assumption in the stability analysis.

3.2. *Numerical analysis of stability using generalized body force $\boldsymbol{f}_{ac}$*

Thus far, in the theoretical stability analysis (§ 2) as well as in the numerical simulations (§ 3.1), a simplified equation for $\boldsymbol{f}_{rl}$ (2.4) is employed as a body force with the assumption of constant E_{ac} (the amplitudes p_a and v_a of first-order fields p_1 and v_1 do not vary during relocation). In this section, the generalized acoustic body force $\boldsymbol{f}_{ac}$ in (2.2) is employed and the first-order fields required to calculate the above $\boldsymbol{f}_{ac}$ are obtained from the wave equations (frequency domain – see Appendix A) by actuating the channel walls at a frequency ν with a wall displacement d_0. There are two reasons for using a generalized acoustic body force $\boldsymbol{f}_{ac}$. (1) To show the relocation predicted by $\boldsymbol{f}_{rl}$ and $\boldsymbol{f}_{ac}$

is approximately the same. When we use much simpler $\boldsymbol{f}_{rl}$ instead of the complex $\boldsymbol{f}_{ac}$, the first-order field equations are not required to be solved which will significantly reduce the computation time for simulation of relocation of inhomogeneous fluids. (2) To explain the previous microchannel experiments in immiscible fluid relocation (Hemachandran *et al.* 2019).

For one-dimensional (1-D) standing half-wave simulations, the sidewalls are actuated in phase at a displacement d_0 at a frequency ν. In laminar flow equations, the boundary conditions used are no-slip at all walls, and the pressure is constrained at a point (bottom left corner of the channel). To disregard the effect of streaming, the first-order acoustic fields are allowed to slip in the frequency domain.

Figure 6(a) shows the HLH configuration subjected to a 1-D standing half-wave by actuating sidewalls at a displacement d_0 of 0.21 nm and a frequency ν of 1.73 MHz. In this case, it is observed that the resulting pressure amplitude P_a of 0.67 MPa ($E_{ac} =$ 85.58 J m^{-3}) could not relocate the fluids in the HLH configuration and thus remains stable. However, when the displacement is increased to 0.22 nm, the resulting pressure amplitude of $P_a = 0.69$ MPa ($E_{ac} = 86.22$ J m^{-3}) could relocate the HLH configuration to a stable equilibrium, as shown in figure 6(b). The value of E_{cr} (86.22 J m^{-3}) obtained through a generalized body force $\boldsymbol{f}_{ac}$ (where the variation of pressure field in each fluid is taken into account) is in close agreement with E_{cr} (88.78 J m^{-3}) obtained by the simplified relocation force $\boldsymbol{f}_{rl}$ (where the assumptions of homogeneous p_1, v_1 and steady E_{ac} are involved). From the above discussion, it is evident that for fluids with an impedance difference as large as 24.91 % (mineral–silicone oil), the deviation in critical acoustic energy density (E_{cr}) predicted by theoretical stability analysis and generalized body force $\boldsymbol{f}_{ac}$ is found to be only 3.22 %. Thus, the assumption of homogeneous p_1 and v_1 and steady E_{ac} employed in theoretical analysis holds.

In the case of a 1-D standing half-wave, when the interface of the fluid coincides with the pressure node ($x_s = 0$), for any E_{ac}, relocation is not observed using both $\boldsymbol{f}_{ac}$ and $\boldsymbol{f}_{rl}$ (figures 3c and 4c) as predicted by the stability criteria in (2.21). However, Hemachandran *et al.* (2019) through experiments demonstrated the relocation of fluids irrespective of the location of the vertical interface x_s. In their experiments, the frequency employed (2.1 MHz) is far from the 1-D resonant half-wave frequency ($\nu = 1.6$ MHz $\approx c_{avg}/2w$). In our previous work (Rajendran *et al.* 2022), we have shown that the above relocation is due to standing two-dimensional (2-D) acoustic wave (frequency $\nu = 2.1$ MHz between $c_{avg}/2w$ and $c_{avg}/2h$) as shown in figure 4(d). From figure 4(d) it is clear that the pressure node is not vertical but inclined with respect to the fluid interface owing to the 2-D actuation (all four walls are actuated at d_0). The above 2-D relocation can be clearly explained by the fact that if the fluid interface and node are not perpendicular to each other, then $\nabla \times \boldsymbol{f}_{rl} \neq 0$. This implies that when a sufficient energy density is applied, the fluid system in figure 4(d) will not be in equilibrium and relocation begins without imposing any perturbations unlike the other relocation discussed in this work.

3.3. *Characterization of stable and unstable (relocation) regime*

When the 1-D acoustic standing wave is imposed on fluids with interfacial tension, the configurations (figures 1b, 2b-i and 3a) having high impedance fluid at the anti-node and low impedance fluid at the node, become conditionally stable. From (2.21), it is evident that the stability of the above inhomogeneous fluid configurations is governed by the ratio of F_{rl} and F_{int}, which is called the acoustic Bond number (Bo_a) similar to other acoustic

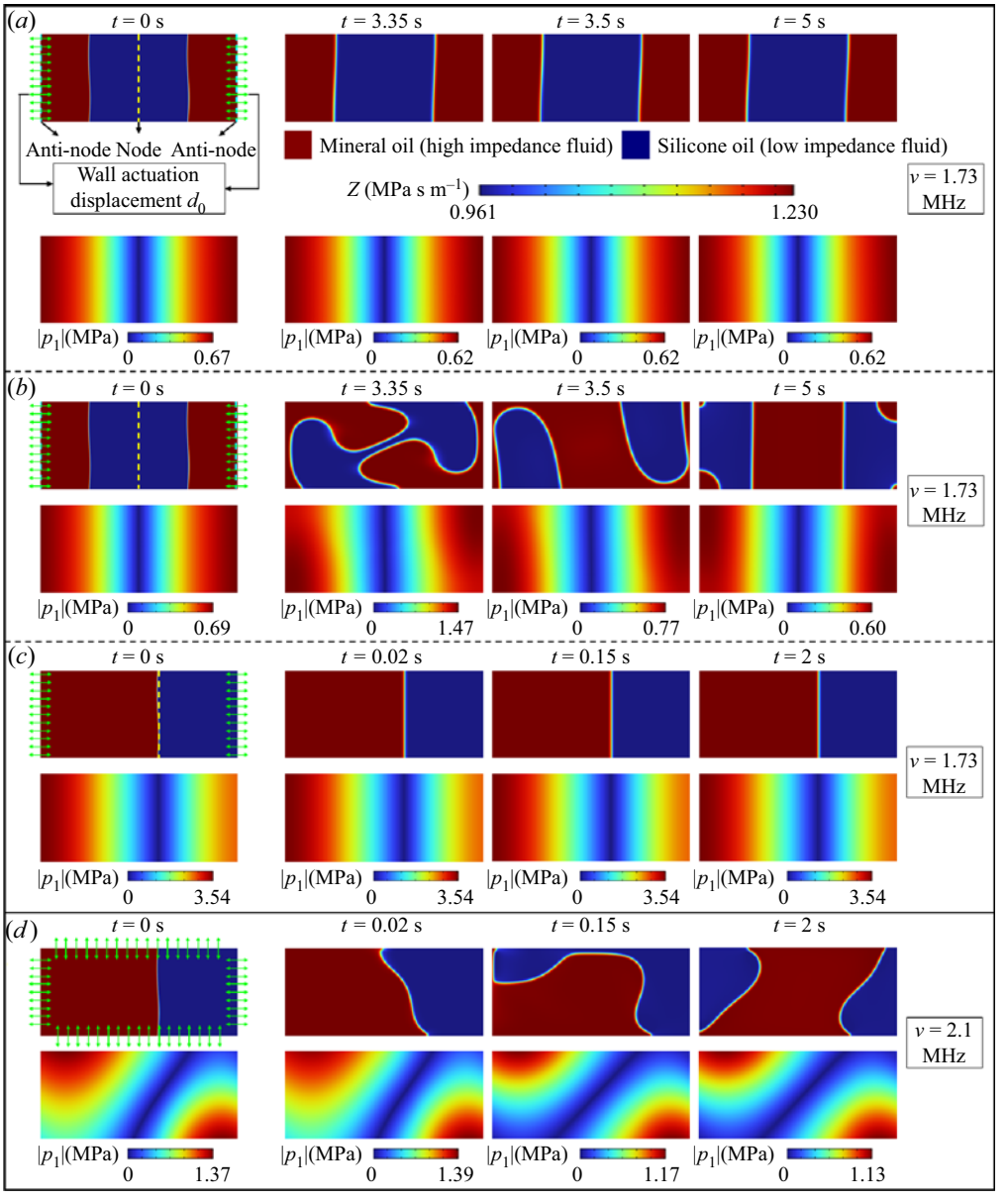

Figure 4. Stabilization and relocation of inhomogeneous fluids using generalized body force $\boldsymbol{f}_{ac}$ in (2.2) along with the first-order pressure field ($|p_1| = \sqrt{real(p_1^{\star} p_1)}$) for different fluid configurations. One-dimensional (1-D) actuation is imposed on configurations shown in (*a–c*), and two-dimensional (2-D) actuation is imposed on configurations shown in (*d*). (*a*) HLH configuration remains stable up to $E_{ac} = 85.58$ J m^{-3} ($p_a = 0.67$ MPa, $d_0 = 0.21$ nm, $\nu = 1.73$ MHz). (*b*) HLH configuration undergoes relocation above $E_{ac} = 86.22$ J m^{-3} ($p_a = 0.69$ MPa, $d_0 = 0.22$ nm, $\nu = 1.73$ MHz). Significant variation in $|p_1|$ during relocation is observed. (*c*) HL configuration where the fluid interface coincides with the node remains in stable equilibrium even at $E_{ac} = 2334$ J m^{-3} ($p_a = 3.54$ MPa, $d_0 = 20$ nm, $\nu = 1.73$ MHz). (*d*) Relocation of HL configuration due to 2-D wall actuation ($p_a = 1.37$ MPa, $d_0 = 20$ nm, $\nu = 2.1$ MHz).

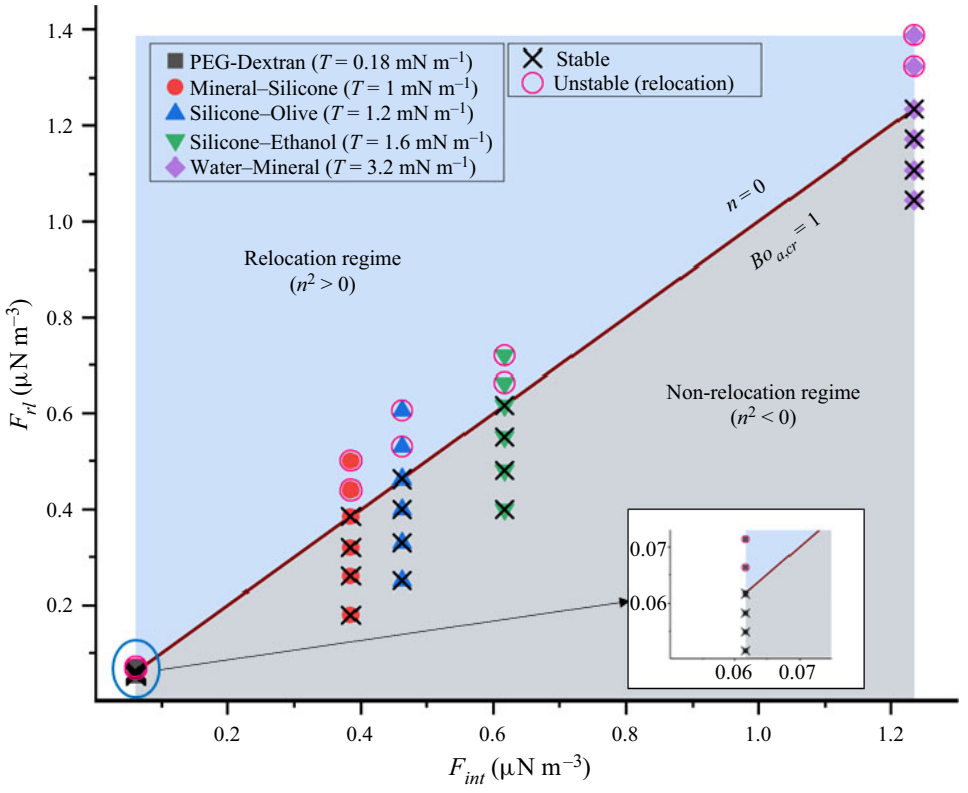

Figure 5. Characterization of relocation and non-relocation regimes of immiscible HLH fluid configuration using acoustic Bond number Bo_a and characteristic value n. The blue and grey colours indicate the theoretically predicted relocation regime ($n^2 > 0$ or $Bo_a > 1$: unstable) and non-relocation regime ($n^2 < 0$ or $Bo_a < 1$: stable), respectively. The line separating these two regimes indicates a neutral configuration ($n = 0$ or $Bo_a = 1$). The data points are obtained through numerical simulations where the open circle indicates relocation and the cross mark indicates non-relocation.

dimensionless numbers (Mitas, Manor & Thiele 2021; Muñoz *et al.* 2021):

$$Bo_a = \frac{F_{rl}}{F_{int}} = \frac{\phi E_{ac} \Delta Z \sin(2k_w x_s)}{k_h^2 T}. \tag{3.1}$$

The Bo_a that separates the stable and unstable region is called the critical acoustic Bond number $Bo_{a,cr}$. From (2.21),

$$Bo_{a,cr} = 1. \tag{3.2}$$

For $Bo_a > Bo_{a,cr}$, the above configurations become unstable (relocation occurs) and for $Bo_a < Bo_{a,cr}$, the configurations remain stable. Figure 5 shows the simulation results of different immiscible fluid combinations. The relocation and non-relocation regimes predicted by the simulations are in line with (3.2). It must also be noted that the fluids with higher interfacial tension require a higher acoustic force for relocation.

3.4. *Effect of the height of the channel on stability*

The height of the channel h plays a critical role in the stability of immiscible fluids. For a given E_{ac}, the increase in h weakens the stabilizing effect of the interfacial tension

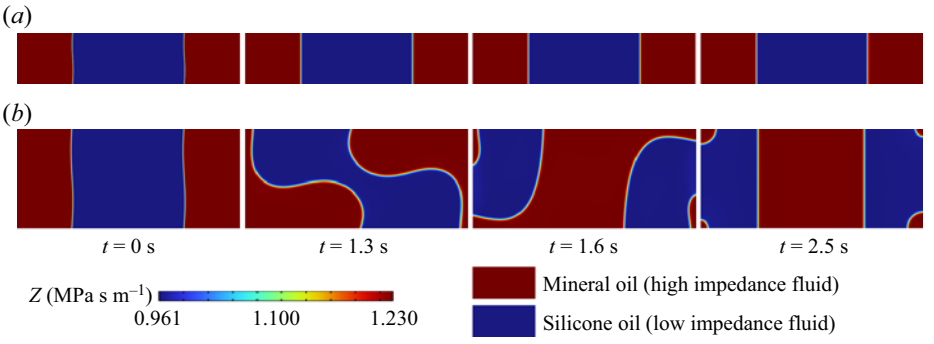

Figure 6. Effect of channel height on stability: (*a*) channel height $h = 80$ μm – no relocation is observed as applied energy density ($E_{ac} = 120$ J m^{-3}) is less than the critical energy density ($E_{cr} = 384$ J m^{-3}); (*b*) channel height $h = 160$ μm – relocation is observed as applied energy density ($E_{ac} = 120$J m^{-3}) is high than the critical energy density ($E_{cr} = 88.78$ J m^{-3}). This demonstrates that the interfacial tension force weakens as the height of the channel increases and thus a higher height of the channel results in a lower E_{ac} required for relocation as ($E_{cr} \propto 1/h^2$).

force, as analysed theoretically in § 2. From (2.22), it can be inferred that the critical acoustic energy density is inversely proportional to the square of the channel height ($E_{cr} \propto 1/h^2$). In figure 6(*a*), for a microchannel of height $h = 80$ μm consisting of mineral–silicone oil with an interfacial tension $T = 1$ mN m^{-1}, the fluid system is stable as the applied E_{ac} (120 J m^{-3}) is lower than the critical energy density ($E_{cr} = 384$ J m^{-3}). However, for $h = 160$ μm and keeping the remaining parameters the same, fluid relocation is observed as the applied E_{ac} (120 J m^{-3}) is higher than the critical energy density ($E_{cr} = 88.78$ J m^{-3}).

The above discussion on the effect of channel height on acoustic relocation has high relevance in practical applications. To relocate fluids with a high interfacial tension of ($O(10^1$mN m^{-1}–10^2 mN m^{-1})), in commonly used acoustofluidic channels of height (depth) ranging from 100 μm to 200 μm, the required E_{ac} becomes $\approx O(10^4)$ J m^{-3}, which is very high compared with the E_{ac} employed in typical acoustofluidic experiments ($O(10^2$ J m^{-3}–10^3 J m^{-3})). Equation (2.22) tells that the above problem can be solved by increasing the channel height as $E_{ac} \propto 1/h^2$. Hence, the height (depth) of the channel is a crucial aspect to be considered during the fabrication of an acoustofluidic microchannel for handling high interfacial tension fluids.

4. Conclusion

We have theoretically established the stability criteria for inhomogeneous fluids subjected to standing acoustic fields, which is consistent with the previous experimental investigations on miscible (Deshmukh *et al.* 2014; Karlsen *et al.* 2016) and immiscible fluids (Hemachandran *et al.* 2019). Numerical simulations using a simplified and generalized acoustic body force were carried out to understand the various parameters that contribute towards the stability and relocation of fluids. However, the effect of viscous boundary layer-driven acoustic streaming on relocation is neglected in this work, which will be addressed in an upcoming paper. The insights gained from this study can have potential applications in inhomogeneous fluid handling and particle manipulation in the field of acoustofluidics.

Funding. This work was supported by the Department of Science & Technology – Science and Engineering Research Board (DST-SERB) via grant no. SRG/2021/002180 and the Department of Science and Technology – Fund for Improvement of Science and Technology Infrastructure (DST-FIST) via grant no. SR/FST/ET-I/2021/815.

Declaration of interests. The authors report no conflict of interest.

Author ORCIDs.
Karthick Subramani https://orcid.org/0000-0002-7751-7759.

Appendix A. First-order fields in the frequency domain

The first-order fields (fast time scale) on the frequency domain are written as

$$-\mathrm{i}\omega\rho_1 = \boldsymbol{\nabla}\cdot(\rho\boldsymbol{v}_1), \tag{A1a}$$

$$-\mathrm{i}\omega\rho\boldsymbol{v}_1 = -\boldsymbol{\nabla}p_1 + \eta\nabla^2\boldsymbol{v}_1 + \beta\eta\boldsymbol{\nabla}(\boldsymbol{\nabla}\cdot\boldsymbol{v}_1), \tag{A1b}$$

$$-\mathrm{i}\omega\rho\kappa p_1 = -\mathrm{i}\omega\rho_1 + \boldsymbol{v}_1\cdot\boldsymbol{\nabla}\rho. \tag{A1c}$$

Also, combining (A1*a*) and (A1*c*), we get

$$-\mathrm{i}\omega\kappa p_1 = -\boldsymbol{\nabla}\cdot\boldsymbol{v}_1, \tag{A1d}$$

where p_1 is the first-order pressure field, ρ_1 refers to first-order density field, $\boldsymbol{v}_1$ is the first-order velocity field, ρ is the slow time scale density, κ is the slow time scale compressibility, ω is the angular frequency, η is the dynamic viscosity of the fluid, ξ is the volume fluid viscosity and $\beta = (\xi/\eta) + (1/3)$. The detailed analysis of first-order and second-order fields acting on inhomogeneous fluids is given by Rajendran *et al.* (2022).

References

Ahmed, D., Ozcelik, A., Bojanala, N., Nama, N., Upadhyay, A., Chen, Y., Hanna-Rose, W. & Huang, T.J. 2016 Rotational manipulation of single cells and organisms using acoustic waves. *Nat. Commun.* **7**, 11085.

Augustsson, P., Karlsen, J.T., Su, H.-W., Bruus, H. & Voldman, J. 2016 Iso-acoustic focusing of cells for size-insensitive acousto-mechanical phenotyping. *Nat. Commun.* **7** (1), 1–9.

Baudoin, M., Thomas, J.-L., Al Sahely, R., Gerbedoen, J.-C., Gong, Z., Sivery, A., Matar, O.B., Smagin, N., Favreau, P. & Vlandas, A. 2020 Spatially selective manipulation of cells with single-beam acoustical tweezers. *Nat. Commun.* **11**, 4244.

Chandrasekhar, S. 1961 *Hydrodynamic and Hydromagnetic Stability*. Dover.

Christakou, A.E., Ohlin, M., Vanherberghen, B., Khorshidi, M.A., Kadri, N., Frisk, T., Wiklund, M. & Önfelt, B. 2013 Live cell imaging in a micro-array of acoustic traps facilitates quantification of natural killer cell heterogeneity. *Integr. Biol.* **5** (4), 712–719.

Collins, D.J., Morahan, B., Garcia-Bustos, J., Doerig, C., Plebanski, M. & Neild, A. 2015 Two-dimensional single-cell patterning with one cell per well driven by surface acoustic waves. *Nat. Commun.* **6**, 8686.

Deshmukh, S., Brzozka, Z., Laurell, T. & Augustsson, P. 2014 Acoustic radiation forces at liquid interfaces impact the performance of acoustophoresis. *Lab on a Chip* **14** (17), 3394–3400.

Friend, J. & Yeo, L.Y. 2011 Microscale acoustofluidics: microfluidics driven via acoustics and ultrasonics. *Rev. Mod. Phys.* **83** (2), 647–704.

Gautam, G.P., Gurung, R., Fencl, F.A. & Piyasena, M.E. 2018 Separation of sub-micron particles from micron particles using acoustic fluid relocation combined with acoustophoresis. *Anal. Bioanal. Chem.* **410** (25), 6561–6571.

Hemachandran, E., Hoque, S.Z., Laurell, T. & Sen, A.K. 2021 Reversible stream drop transition in a microfluidic coflow system via on demand exposure to acoustic standing waves. *Phys. Rev. Lett.* **127** (13), 134501.

Hemachandran, E., Karthick, S., Laurell, T. & Sen, A.K. 2019 Relocation of coflowing immiscible liquids under acoustic field in a microchannel. *Europhys. Lett.* **125** (5), 54002.

HOQUE, S.Z. & SEN, A.K. 2023 Ultrasound resonance in coflowing immiscible liquids in a microchannel. *Phys. Rev.* E **107** (3), 035104.

IRANMANESH, I., RAMACHANDRAIAH, H., RUSSOM, A. & WIKLUND, M. 2015 On-chip ultrasonic sample preparation for cell based assays. *RSC Adv.* **5** (91), 74304–74311.

JAYAKUMAR, S. & SUBRAMANI, K. 2022 An investigation of acoustic relocation phenomenon in a microchannel under acoustic fields. *Phys. Fluids* **34** (9), 092002.

KARLSEN, J.T., AUGUSTSSON, P. & BRUUS, H. 2016 Acoustic force density acting on inhomogeneous fluids in acoustic fields. *Phys. Rev. Lett.* **117** (11), 114504.

KARLSEN, J.T. & BRUUS, H. 2017 Acoustic tweezing and patterning of concentration fields in microfluidics. *Phys. Rev. Appl.* **7** (3), 034017.

KARLSEN, J.T., QIU, W., AUGUSTSSON, P. & BRUUS, H. 2018 Acoustic streaming and its suppression in inhomogeneous fluids. *Phys. Rev. Lett.* **120** (5), 054501.

KARTHICK, S. & SEN, A.K. 2018 Improved understanding of acoustophoresis and development of an acoustofluidic device for blood plasma separation. *Phys. Rev. Appl.* **10** (3), 034037.

LAKSHMANAN, A., JIN, Z., NETY, S.P., SAWYER, D.P., LEE-GOSSELIN, A., MALOUNDA, D., SWIFT, M.B., MARESCA, D. & SHAPIRO, M.G. 2020 Acoustic biosensors for ultrasound imaging of enzyme activity. *Nat. Chem. Biol.* **16**, 988–996.

LANDAU, L.D. & LIFSHITZ, E.M. 1987 *Fluid Mechanics*. Pergamon.

LI, P., *et al.* 2015 Acoustic separation of circulating tumor cells. *Proc. Natl Acad. Sci. USA* **112** (16), 4970–4975.

LU, X., MARTIN, A., SOTO, F., ANGSANTIKUL, P., LI, J., CHEN, C., LIANG, Y., HU, J., ZHANG, L. & WANG, J. 2019 Parallel label-free isolation of cancer cells using arrays of acoustic microstreaming traps. *Adv. Mater. Technol.* **4** (2), 1800374.

MITAS, K.D.J., MANOR, O. & THIELE, U. 2021 Bifurcation study for a surface-acoustic-wave-driven meniscus. *Phys. Rev. Fluids* **6** (9), 094002.

MUÑOZ, J., ARCOS, J., CAMPOS-SILVA, I., BAUTISTA, O. & MÉNDEZ, F. 2021 Slippage effect on interfacial destabilization driven by standing surface acoustic waves under hydrophilic conditions. *Phys. Rev. Fluids* **6** (2), 024002.

NATH, A. & SEN, A.K. 2019 Acoustic behavior of a dense suspension in an inhomogeneous flow in a microchannel. *Phys. Rev. Appl.* **12** (5), 054009.

POTHURI, C., AZHARUDEEN, M. & SUBRAMANI, K. 2019 Rapid mixing in microchannel using standing bulk acoustic waves. *Phys. Fluids* **31** (12), 122001.

RAJENDRAN, V.K., JAYAKUMAR, S., AZHARUDEEN, M. & SUBRAMANI, K. 2022 Theory of nonlinear acoustic forces acting on inhomogeneous fluids. *J. Fluid Mech.* **940**, A32.

RUFO, J., CAI, F., FRIEND, J., WIKLUND, M. & HUANG, T.J. 2022 Acoustofluidics for biomedical applications. *Nat. Rev. Meth. Primers* **2** (1), 30.

SHI, J., HUANG, H., STRATTON, Z., HUANG, Y. & HUANG, T.J. 2009 Continuous particle separation in a microfluidic channelvia standing surface acoustic waves (SSAW). *Lab on a Chip* **9** (23), 3354–3359.

VAN ASSCHE, D., REITHUBER, E., QIU, W., LAURELL, T., HENRIQUES-NORMARK, B., MELLROTH, P., OHLSSON, P. & AUGUSTSSON, P. 2020 Gradient acoustic focusing of sub-micron particles for separation of bacteria from blood lysate. *Sci. Rep.* **10**, 3670.

WU, M., OZCELIK, A., RUFO, J., WANG, Z., FANG, R. & HUANG, T.J. 2019 Acoustofluidic separation of cells and particles. *Microsyst. Nanoengng* **5** (1), 1–18.

XIE, Y., RUFO, J., ZHONG, R., RICH, J., LI, P., LEONG, K.W. & HUANG, T.J. 2020 Microfluidic isolation and enrichment of nanoparticles. *ACS Nano* **14** (12), 16220–16240.

ZHANG, L., TIAN, Z., BACHMAN, H., ZHANG, P. & HUANG, T.J. 2020 A cell-phone-based acoustofluidic platform for quantitative point-of-care testing. *ACS Nano* **14** (3), 3159–3169.